SEA WATER TURBIDITY ANALYSIS FROM SENTINEL-2 IMAGES: ATMOSPHERIC CORRECTION AND BANDS CORRELATION

A. Pisanti[1], S. Magrì[2,3], I. Ferrando[3,*], B. Federici[3]

[1] Department of Earth, Environmental and Life Sciences (DISTAV), University of Genoa,
Corso Europa 26, 16132 Genoa, Italy – alessandra.pisanti@libero.it
[2] Environment State and Protection from Natural Hazards Department,
Regional Agency for the Environmental Protection of Liguria (ARPAL),
via Bombrini 8, 16149 Genoa, Italy – stefania.magri@arpal.liguria.it
[3] Department of Civil, Chemical and Environmental Engineering (DICCA), University of Genoa,
via Montallegro 1, 16145 Genoa, Italy – ilaria.ferrando@edu.unige.it, bianca.federici@unige.it

Commission IV, WG IV/4

KEY WORDS: Sea water turbidity, Earth Observation, Sentinel-2, atmospheric correction, bands correlation, Aerosol Optical Depth

ABSTRACT:

Turbidity is a visual property of water, related to the presence of suspended particles in waters. This parameter is measured in different water quality monitoring programmes as it can determine negative environmental effects both on the biotic and abiotic marine ecosystem. Traditional methods, e.g., in situ monitoring, offer high accuracy but provide sparse information in space and time. On the other hand, Earth Observation (EO) techniques have the potential to provide a comprehensive, fast and inexpensive monitoring system to observe the biophysical and biochemical conditions of water bodies. In the present work, a method for seawater turbidity retrieval from Sentinel-2 multispectral optical images, freely available within the EU Copernicus programme, is presented. The study explores different atmospheric correction methods available in open source software (QGIS, GRASS GIS and SNAP), in order to convert Level-1C (L1C) Top-Of-Atmosphere (TOA) images to Level-2A (L2A) Bottom-Of-Atmosphere (BOA), when the latter is not directly available. Once the proper method for atmospheric correction was identified and applied, the correlation between the in situ dataset and the individual bands known to be most sensitive to water turbidity, i.e., blue (B2), green (B3), red (B4) and near infrared (B8 and B8A) bands, were investigated and a linear regression model between selected band values and turbidity was identified.

1. INTRODUCTION

Turbidity is a visual property of water and is a measure of the amount of light scattered by particles in water. It is due to the presence of suspended particles, i.e., suspensoids, which operationally can be defined as the fraction in water that can be removed by a pore size filter of 0.22 μm (Kirk, 1985). Generally, increases in the concentration of algae and organic matter cause an increase in turbidity, but higher turbidity events are dominated by high concentrations of inanimate inorganic particles (Myint and Walker, 2002; Lee et al., 2015). Concentration of suspended sediments is largely driven by interactions of different physical forcing such as river discharge, wind speed, tides, precipitation and shoreline erosion. In shallow aquatic systems, strong winds can cause seabed shear stress or mixing events that affect bottom sediments resuspension (Quang et al., 2017; Olds et al., 2011; Joshi et al., 2017). Other sources are represented by anthropogenic activities, such as dredging operations or bottom resuspension from ship propellants. In highly anthropized coastal marine systems, like harbours, sediments represent a sink for contaminants and resuspension can contribute to propagate pollution to unpolluted areas (Lisi et al., 2019).
Turbidity is an important parameter because it affects a variety of aquatic ecosystem processes (Abirhire et al., 2020); indeed, many marine water quality monitoring programmes of EU legislation measure nephelometric turbidity for its significant interest in its multiple effects on aquatic ecosystems (Zampoukas et al., 2013). Traditional methods, as in situ monitoring, offer high accuracy but have shown their constraint due to their time and space limitations. On the other hand, Earth Observation (EO) techniques have the potentiality to provide a comprehensive, fast and inexpensive monitoring system to observe the biophysical and biochemical conditions of water bodies (Caballero et al., 2018; Saberioon et al., 2020; Sagan et al., 2020).
The aim of this study is to develop a semi-empirical model for predicting sea water turbidity along the North Tyrrhenian Sea (Italy), by combining satellite remote sensing data and in situ turbidity measurements.
The turbidity measurements include data from 2015 to 2021, which are collected by ARPAL and by ARPAT, the Regional Agency for the Environmental Protection of Liguria and Tuscany, respectively. Images of Sentinel-2 twin satellites (Sentinel A and B), which have a high spatial and temporal resolution, were processed. They are made freely available and accessible by the EU Copernicus programme. Satellite products are provided at Level-1C (L1C) Top-Of-Atmosphere (TOA) and at Level-2A (L2A) Bottom-of-Atmosphere (BOA). L2A BOA reflectance products are preferred as they are already corrected for effects of the atmosphere. Since the L2A BOA products are available for wider Europe from March 2018 onward, it was necessary to identify the most appropriate method for applying the atmospheric correction to L1C images, in order to use the complete in situ dataset to calibrate the predicting model. Hence, a comparison between the available L2A product and the corresponding L1C image corrected using

* Corresponding author

i.atcorr in GRASS GIS (GRASS Development Team, 2022a,b), the *Sen2Cor* processor in the Sentinel Application Platform (SNAP) ver. 8.0.0 (Lantzanakis et al., 2017; European Space Agency, 2020) and the Semi-Automatic Classification Plugin (Congedo, 2021) in QGIS (QGIS Development Team, 2022) was performed. Both image-based method, i.e., the Dark Object Subtraction (DOS) method (Chavez, 1988) in QGIS, and physically-based methods, i.e., the Second Simulation of Satellite Signal in the Solar Spectrum (6S) method (Vermote et al., 1997; Roger et al., 2022) in *i.atcorr* and *Sen2Cor*, were applied. The great advantage of the DOS method is that it doesn't require remote or in situ atmospheric measurements, but it uses only the spectral and radiometric characteristics of the processed image. The performed correction is usually not so accurate. Instead, the physically-based approach requires atmospheric measurements and parameters, that are difficult to be estimated so to be coherent in space and time with the processed image. The most complex physical parameter to set is Aerosol Optical Depth (AOD), a dimensionless parameter that represents the amount of aerosol in the vertical column of the atmosphere over a target station.
Once the most appropriate method for atmospheric correction was identified, it was applied to the L1C images relative to the collected field data from April 2015 to March 2018. Hence, the correlation between the in situ measurements and the individual bands known to be most sensitive to water turbidity, i.e., blue (B2), green (B3), red (B4) and near infrared (NIR B8 and B8A) bands, was analysed, finding a good correlation for the visible bands and a weak one for NIR bands. Finally, indexes defined by the ratio between the visible bands were calculated and a linear regression model to retrieve sea water turbidity from Sentinel-2 images was identified.

2. MATERIALS AND METHODS

Satellite remote sensing instruments can obtain an optical measurement of water turbidity as it increases the backscattering of light. Indeed, the presence, the concentrations and the types of materials and substances in water highly influence reflection, absorption, and transmittance of electromagnetic radiation (Hafeez et al., 2018). Energy reflected from objects in water at a variety of different wavelengths will provide their spectral responses, as shown in Figure 1. Each type of object has a unique spectral response, also known as spectral signature, which can be used to identify the surface features and their properties (Moore, 1980). In general, clear waters have low reflectance in the green, blue and red bands, and have no reflection in NIR spectrum. High concentrations of suspended sediments in water cause high reflectance measurements in red and NIR bands because they block the transmittance from and to lower depths. High reflectance measurements in green band show a correlation with chlorophyll concentrations and high absorption in blue and red bands due to photosynthetic activity (Figure 1). Remote sensing offers considerable advantages for the study of large areas, the determination of current and circulation patterns, the monitoring of sedimentation, the water productivity, and the eutrophication (Moore, 1980). In this study, the satellite remote sensing is used to capture the response of the electromagnetic interaction with water to estimate turbidity. ESA Sentinel-2 is a multi-spectral and high-resolution imaging mission. The images cover 13 spectral bands from visible to short wave infrared wavelength, from 10 to 60 m spatial resolution. Level-1C (L1C) Top-Of-Atmosphere (TOA) and Level-2A (L2A) Bottom-of-Atmosphere (BOA) products are made

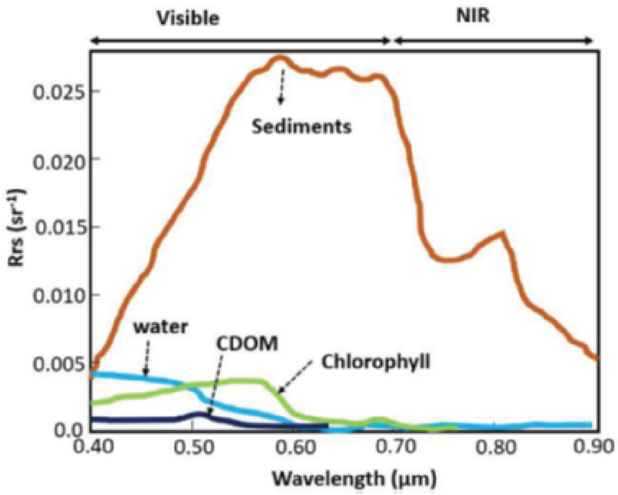

Figure 1. Spectral signatures of water with sediments (orange), clear water (blue), water with chlorophyll content (green), water with Chromophoric Dissolved Organic Matter - CDOM (black). Rrs is the reflectance registered by the sensor. Source: Hafeez et al. (2018).

available to users. The L1C products are the result of radiometric and geometrical corrections. The L2A products are obtained through the atmospheric correction applied to the L1C products and the measurements are given in BOA reflectance. L2A products are available for the whole of Europe from March 2018 onward. Both L1C and L2A products are 100×100 km^2 ortho-images (called tiles) in WGS84/UTM projection[1].
In order to develop a semi-empirical model for predicting sea water turbidity by combining the reflectance measurements in the aforementioned bands, satellite remote sensing data and in situ turbidity measurements have to be aligned. The turbidity measurements in the area under investigation, described in the following section 2.1, include data from 2015 to 2021. Therefore, Sentinel-2 L2A BOA images from March 2018 onward has to be integrated with L1C TOA images from 2015 to 2018, to which atmospheric correction has to be applied after careful verification of the most appropriate method and parameters, as described in section 2.2.

2.1 Case study

For the present study, in situ turbidity data acquired by the Regional Agency for the Environmental Protection of Liguria (ARPAL) and Tuscany (ARPAT) were used. ARPAL and ARPAT are in charge of water quality monitoring for the Liguria and Tuscany Regions, respectively, according to 2000/60/EC Water Quality Directive, implemented in Italy with D.Lgs. 152/2006, and EU Marine Strategy Framework Directive (MSFD), implemented in Italy with D.Lgs 190/2010. The study area covers the coastline from the Marine Protected Area of Cinque Terre (Liguria) until Livorno (Tuscany) and it is entirely contained in Sentinel-2 tile T32TNP. Figure 2 shows the study area and the monitoring stations. In each station, chemical and physical parameters of water column are monitored with different frequency using the multiparameter probe. This instrument allows the acquisition along the water column of temperature, salinity, conductivity, pH, redox potential, dissolved oxygen, Chlorophyll-a and turbidity. Turbidity

[1] https://sentinels.copernicus.eu/web/sentinel/user-guides/sentinel-2-msi

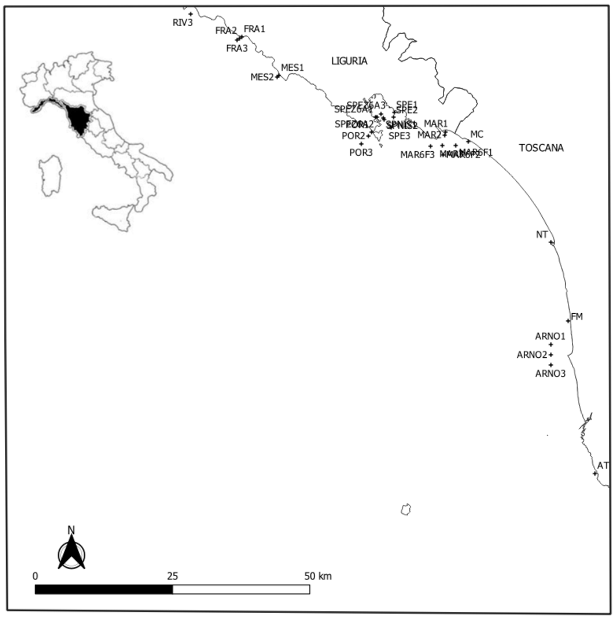

Figure 2. Monitoring stations within the study area.

was measured in nephelometric turbidity units (NTU). At each station, turbidity profiles were conducted from the surface to the bottom, the average value at 0.5 m from the surface was used for the present study. Turbidity measurements include data from 2015 to 2021 and considered values range from 0.2 NTU to 28.7 NTU.

2.2 Atmospheric correction

The signal received by the sensor is composed by both the radiance of the target and atmospheric effects, because each electromagnetic signal interacts with the atmosphere of the Earth (Teillet, 1986). The process used to remove the quantitative contribution of the atmosphere from the signal received at the satellite sensor is called "atmospheric correction". Atmospheric correction is one of the key steps in remote sensing, which influences the final image. For this reason, many techniques and algorithms within several software have been developed over time. Atmospheric correction methods can be divided into two main groups (Hadjimitsis et al., 2004): image-based approach and physically-based approach.
Image-based approaches focus on the spectral and radiometric characteristics of the processed image from which the atmospheric effects are derived and subtracted to the TOA reflectance in order to obtain the BOA reflectance. An example of image-based approach is the Dark Object Subtraction (DOS).
The DOS model is based on the lower value of reflectance (darker objects) of the image. The identification of that value starts from the presumption that just few pixels of the image should be completely black, but due to the atmospheric effects it's assumed that the radiance received at sensor from these pixels are almost composed of atmospheric scattering (Chavez, 1988). Hence, this method consists in the subtraction of a constant value from each pixel of the processed image, but this value changes depending on the considered image. The greatest advantage of this method is that it doesn't require atmospheric measurements. The disadvantage is that it removes the additive contribution of the scattering effects, while it does not consider the effect of transmittance caused by scattering and absorption (Chavez, 1996).
Physically-based approach requires atmospheric measurements and parameters that must be consistent in space and time with the processed image. This approach relies on the use of a radiative transfer model which accurately computes the atmospheric effects (absorption and scattering) and removes them from the sensor observations to obtain the surface reflectance. An example of physically-based approach is the Second Simulation of Satellite Signal in the Solar Spectrum (6S). The 6S method needs a lot of input parameters, including meteorological visibility or Aerosol Optical Depth (AOD), information of the sensor, sun zenith and azimuth, the sensing date and time of image acquisition, the latitude and longitude of the scene center, a digital elevation model, to cite few. The "exact" solution is still a complex issue because of the several input parameters that have to be spatially and temporally coherent with the observations (Kotchenova et al., 2006).
In general, the physically-based approach is more accurate than the image-based one, but, since the required atmospheric parameters can be unavailable, the image-based approach is more usable (Chavez, 1988, 1996).

2.3 Processing in GIS

There are several Geographic Information System (GIS) software providing many functions and tools for the geo-processing of satellite images. The tested software in this study are the free and open source QGIS and GRASS GIS, and the Sentinel Application Platform (SNAP), provided by ESA/ESRIN.
Among all the QGIS functions and plugins, the Semi-Automatic Classification Plugin (SCP) (Congedo, 2021) should be cited. It allows the supervised classification of remote sensing images and provides tools for the download, the preprocessing and post-processing of images. This plugin is also able to apply the atmospheric correction using the DOS method. The only required inputs are a directory containing Sentinel-2 bands of Level-1C and the corresponding Metadata file (MTD MSI - Multi-Spectral Instrument). The final outputs obtained are thirteen raster files in GeoTIFF format containing the reflectance values for each pixel in a range from 0 to 1. Any outliers will be normalized by SCP tool simply setting them equal to 1.
In GRASS GIS the atmospheric correction is made possible applying the 6S algorithm through the *i.atcorr* module[2], defining input data, parameters and atmospheric models has as follows:

1. input raster map containing the radiance on one band; if the input raster map contains reflectance, -r flag should be used;
2. output rescale (e.g. 0,1 or 0,255);
3. geometrical conditions of the sensor, coded with specific numbers (e.g., 25 for Sentinel-2A and 26 for Sentinel-2B);
4. month, day, decimal hours in Greenwich Mean Time (GMT), decimal longitude and latitude of the image center;
5. standard atmospheric model, associated with coded numbers (e.g., 0 for No Gaseous Absorption, 1 for Tropical, 2 for Mid-latitude Summer, etc.);
6. standard aerosols model, available and coded with numbers (e.g., 0 for No Aerosol, 1 for Continental Model, 2 for Maritime Model, etc.);
7. aerosol concentration model (visibility): if an estimate of the meteorological visibility is available, it has to be

[2] https://grass.osgeo.org/grass78/manuals/i.atcorr.html

entered and expressed in km; otherwise the parameter has to be set equal to 0 and the AOD at 550nm has to be indicated;

8. mean target elevation above sea level (e.g., 0 means the target is at the sea level, otherwise it has to be added as a negative value expressed in km);
9. height sensor in km, where 0 means that the sensor is at the ground level and -1000 means that the sensor is on board a satellite;
10. sensor band, using a code for each band of pre-defined satellites (e.g. for Sentinel-2A the blue band has code 167, the green band 168, the red band 169, etc.).

The most difficult parameters to set is the AOD (Roger et al., 2022), a dimensionless parameter related to the amount of aerosol in the vertical column of the atmosphere over the target station. It ranges from 0 to 1; values lower than 0.1 correspond to a clean atmosphere with high visibility, and values higher than 0.4 correspond to hazy atmosphere with very low visibility. This parameter can be estimated from the Aerosol Robotic Network (AERONET)[3], a federation of ground-based globally distributed remote sensing aerosol networks with more than 25 years of data. From the data visualisation interface of the AERONET website, it is possible to search for the nearest measurement site or one with atmospheric characteristics potentially closest to the site under study. Then, it is necessary to look for the AOD value at 550 nm and at the same time as the satellite image was taken. Level 2.0 data products are suggested, because pre- and post-field calibrated, cloud-screened, and quality-assured data (Giles et al., 2019).
The *i.atcorr* module processes one band at time, therefore it has to be run for each one. The final outputs are thirteen raster files, normalized and rescaled within the defined output range defined in input.
The Sentinel Application Platform (SNAP) is an architecture for all Sentinel processing and analysis. It's published under the GPL license and with its sources code available on GitHub. The algorithm used by ESA for atmospheric correction of TOA Level-1C input data is named *Sen2Cor* (Louis et al., 2016). It is a physically-based approach and is dependent on the computation of radiative transfer functions for different sensor and solar geometries, ground elevations and atmospheric parameters. The processor reads the parameter in form of Look Up Tables (LUTs) pertaining to this parameter space and interpolates, if required. The LUTs have been generated via *libRadtran*, a library for the calculation of solar and thermal radiation in the Earth atmosphere. *Sen2Cor* needs the input of the directory containing the metadata file (MTD MSI) of the satellite image and the LUTs can be automatically determined by the processor, or they can be configurable by the user in the configuration file L-2A *GIPP.xml* located in the *cfg* folder of the subdirectory of the processor.
The atmospheric correction can be obtained changing few parameters of the L2A *GIPP.xml* with respect to the default ones:

1. DEM reference: the processor will start automatically to download the DEM from the chosen database;
2. Aerosol type: there are two different types of aerosols (rural and maritime). If set "auto", it can be automatically determined by the processor;
3. Midlatitude: there are two different types of midlatitude (summer and winter). If set "auto", it can be automatically determined by the processor;
4. Cirrus correction: it can be set as "true" or "false". If set to "true", the correction is applied.

2.4 Bands correlation

The correlation between measured turbidity in situ and the surface reflectance in the raster cell in the position of the measuring station was investigated for the different bands, using L2A products when available, i.e., from 2018 to 2021, and L1C products corrected of the effect of the atmosphere from 2015 to 2018. For water quality assessment the blue, green, red and NIR bands are commonly used (Wang et al., 2006; Nas et al., 2010; Gholizadeh et al., 2016). A review of band correlation was proposed by Abirhire et al. (2020), as shown in Table 1, where CA is coastal/aerosol band, B, G, R and NIR are blue, green, red and near infrared bands, respectively.

3. RESULTS

The study explored first of all the spatial and temporal AOD variability and its effect on the atmospheric correction method available in GRASS GIS. Hence a comparison between the atmospheric correction applied by QGIS, GRASS GIS and SNAP was performed for images available both at Level-1C (TOA) and Level-2A (BOA). Once the proper method for atmospheric correction was identified and applied, the correlation between the in situ dataset and the individual bands known to be most sensitive to water turbidity were investigated and a linear regression model between selected band values and turbidity was identified, as detailed in the following.

3.1 AOD variability and its influence on i.atcorr

The evaluation of AOD variability in time and space was analysed for the study area and the year 2020. The following AERONET stations were selected taking into account many factors: altitude, latitude, proximity and distance from the coastline:

1. Palma de Mallorca, Spain (altitude of 10 m)
2. CeSMA, Naples, Italy (altitude of 50 m)
3. La Sapienza, Rome, Italy (altitude of 75 m)
4. Modena, Italy (altitude of 125 m)
5. Ispra, Varese, Italy (altitude of 235 m)

The first three stations are located near the coast, with a low altitude but far from the study area; the last two are not situated near to the sea and they have a quite high altitude, but they are closer to the study area. In each station measurements are not continuous but are taken in different hours, days and months.
The AOD variability during the day in the different stations could be high, as shown in Figure 3 especially in Modena and Ispra stations; moreover, the measurements in a station often do not cover all the hours of the day, or are not available at all, as happened for Naples station in the considered day of Figure 3. The values of all stations range from about 0.10 to 0.47, but, taking into account the stations characterized by more similar values, i.e. the ones along the coast, the average value is 0.15.
In order to understand how the AOD parameter can influence the application of *i.atcorr* module, various tests were carried out, analysing different days, changing the AOD value and keeping all other parameters constant.
An example of the syntax of *i.atcorr* is as follows:
i.atcorr -r input=B04_11082020 range=1,10000 parameters=C:[...]\grassdata\11082020_b4.txt

[3] https://aeronet.gsfc.nasa.gov/new_web/aerosols.html

Table 1. Turbidity models and validation considering several studies (adapted from Abirhire et al., 2020). NTU, FNU and FTU stand for Nephelometric Turbidity Units, Formazin Nephelometric Units, and Formazin Turbidity Units, respectively. B, G, R and N are blue, green, red and near infrared bands, respectively. CA is coastal/aerosol band.

Study System	Units	Sensors	Model	Validation (r^2_{adj})	References
Bow River, Canada	NTU	Landsat-5 TM	$-44.608+1005{\cdot}R$	0.83	Akbar et al., 2014
Lake Beysehir, Turkey	NTU	Landsat-5 TM	$-0.221-0.463{\cdot}B+0.722{\cdot}G+0.841{\cdot}R$	0.6	Nas et al., 2010
Tseng-Wen and Nan-Hwa reservoirs, Taiwan	NTU	Landsat-8 OLI	$4.21-74.26{\cdot}B-14.84{\cdot}G+267.45{\cdot}R-126.89{\cdot}N$	0.73	Liu and Wang, 2019
Missouri and Mississippi Rivers, USA	FNU	Landsat-5 TM	$-156.7+9.020{\cdot}e^{N/B}+154{\cdot}e^{N/G}-83.77{\cdot}e^{N/R}$	0.66	Pereira et al., 2018
		Landsat-7 ETM+	$-59.8+16.9{\cdot}e^{N/B}+163.8{\cdot}e^{N/G}-133.4{\cdot}e^{N/R}$	0.64	
		Landsat-8 OLI	$-138.2+1718{\cdot}e^{N/R}+695.1{\cdot}e^{N/R}$	0.79	
Lake Diefenbaker, Canada	NTU	Landsat-7 ETM+	$3.8531+60.6466{\cdot}R-1.0279{\cdot}R/N-4.7471{\cdot}N/G$	0.91	Abirhire et al., 2020
		Landsat-8 OLI	$-1.3790+55.3844{\cdot}N+6.4725{\cdot}R/G-5.6511{\cdot}N/G$	0.91	
Apalachicola Bay, USA	NTU	Landsat-5 TM	$6568.23{\cdot}R^{1.95}$	0.7	Joshi et al., 2017
Cam Ranh Bay and Thuy Trieu Lagoon, Vietnam	FTU	Landsat-8 OLI	$-1.7826+380.32{\cdot}R$	0.84	Quang et al., 2017
Saint John River, Canada	NTU	Landsat-8 OLI	$-35.420+503.713{\cdot}CA-103.452{\cdot}R$	0.73	El Din, 2021

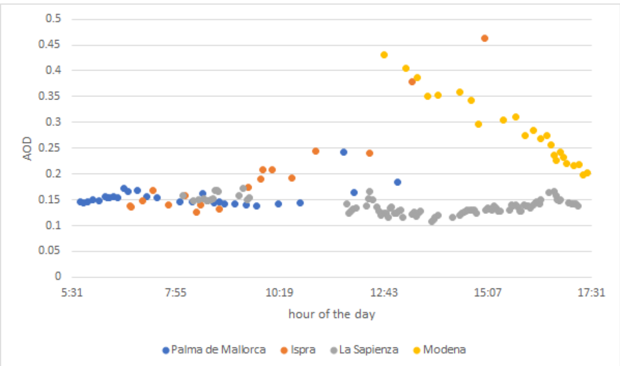

Figure 3. Example of AOD variability during the day in the different stations.

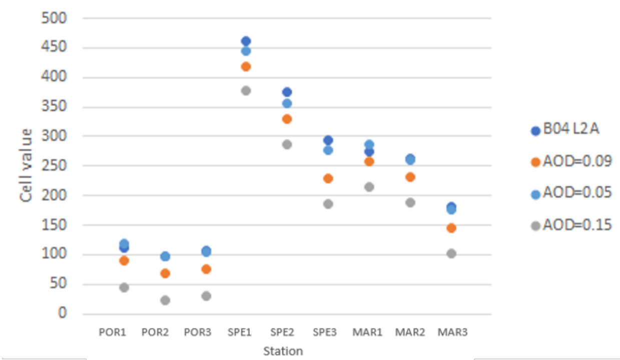

Figure 4. Comparison between L2A reflectance and L1C values corrected using *i.atcorr* and different AOD values in corrispondence at in situ stations and for the red band.

output=B04_11082020_atcorr rescale=0,1
where the parameters file contains: 26 for Sentinel-2B, month, day, hours, longitude and latitude of the image center, mid-latitude summer atmospheric model, maritime areosol model, no aerosol concentration model but AOD=0.15, 0 mean target elevation, -1000 height sensor, i.e. the sensor is on board a satellite, and the code of the analysed sensor band.
Figure 4 shows the sensitivity of *i.atcorr* to the AOD value, which can lead to great uncertainty in the corrected L1C products. The estimated value that comes closest to that of the L2A product, considered as ground truth, is that obtained with the AOD value of 0.05. Such value is very far from the value of 0.15, which could be assumed by analysing the observations from the selected ACRONET stations, as shown in Figure 3.

3.2 Comparison of atmospheric correction methods

In order to understand the proper methodology and parameters for applying atmospheric correction, DOS in QGIS, *i.atcorr* module in GRASS GIS, using the best fitting AOD value, and *Sen2Cor* in SNAP were compared.
For *Sen2Cor* the following parameters were set: DEM reference: SRTM, Aerosol type: set "auto", Midlatitude: "auto",

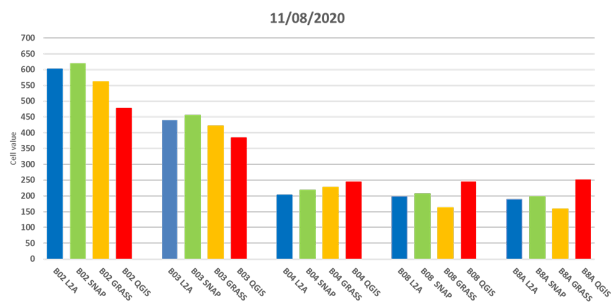

Figure 5. Comparison between L2A products and L1C product corrected in SNAP, GRASS GIS and QGIS software for each analysed band of the day 11 August 2020 (SPE2 station).

Cirrus correction: "true", so to apply the correction.
Figure 5 shows an example of the comparison between L2A products and L1C corrected products for visible bands (B2, B3 and B4, representing blue, green and red bands, respectively) and NIR bands (B8 and B8A) for a specific day and in situ sta-

tion. Results show that the products corrected with the DOS model in QGIS are the farther from L2C products; *i.atcorr* and *Sen2Cor* give comparable results, even if the second one seems working better. Moreover the correction in SNAP can be applied automaticaly for all the bands and without defining an AOD value, often difficult to be estimated properly, as showed in the previous section.

3.3 Bands correlation results

L2C products and L1C products corrected by *Sen2Cor* were finally used to investigate the correlation between the in situ dataset and the individual bands known to be most sensitive to water turbidity. Figures 6 shows that the visible bands (B2, B3 and B4) have a higher correlation in terms of R^2, with values equal to 0.42, 0.63 and 0.62 respectively, while NIR values (B8 and B8a) are poorly correlated.

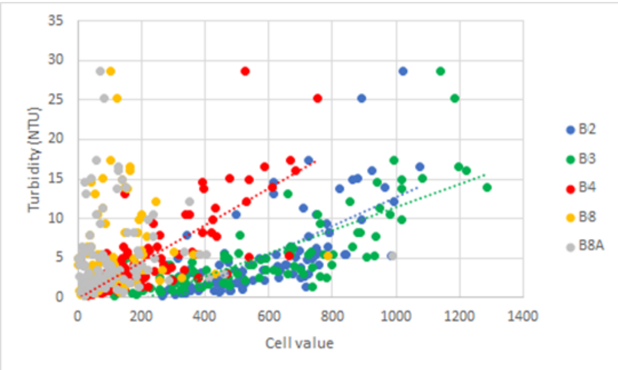

Figure 6. Scatter plot of the turbidity in situ measurements and the respective cell values of the considered bands.

Hence only the visible bands were used to define an index expressing the best correlation to in-situ turbidity measurements, starting from indexes proposed in literature (Abirhire et al., 2020; Wang et al., 2021). The complete dataset includes 102 data from 2015 to 2021, that range from 0.2 NTU to 28.7 NTU. The dataset was split, using a chronological order into a set of about 70% for the model calibration, and the remaining, the most recent, for the model validation phase. The index that shows the best correlation coefficient is:

$$\frac{Rrs(B3) \cdot Rrs(B4)}{Rrs(B2)} \tag{1}$$

where Rrs (B2), Rrs (B3) and Rrs (B4) correspond to the reflectance of blue, green and red bands, respectively.
The identified linear function, in Figure 7, can be expressed as follows:

$$T = 0.0186\frac{Rrs(B3) \cdot Rrs(B4)}{Rrs(B2)} + 0.6276 \tag{2}$$

with a R^2 equal to 0.64. The application of the algorithm to the validation data set shows a determination coefficient value of 0.77, as shown in Figure 8, a RMSE = 2.3 and a MAE = 1.4. Finally, the algorithm was applied to create turbidity maps from the satellite data, using the band calculator in the Semi-Automatic Classification Plugin in QGIS. An example of results is shown in Figure 9.

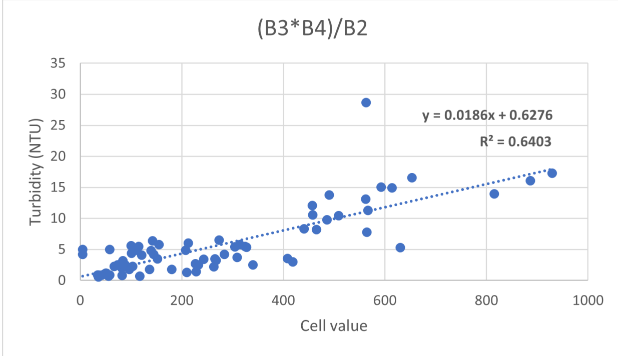

Figure 7. Correlation between the index and the turbidity measurement.

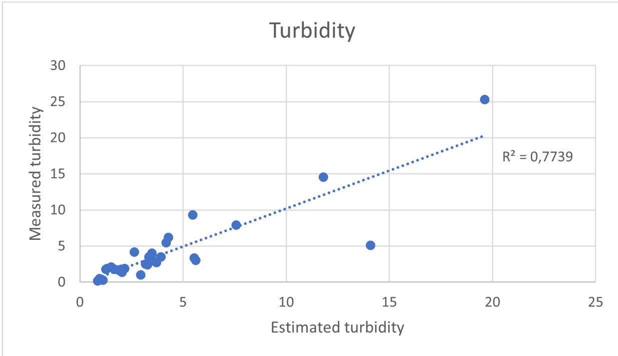

Figure 8. Correlation between the measured turbidity and the estimated turbidity.

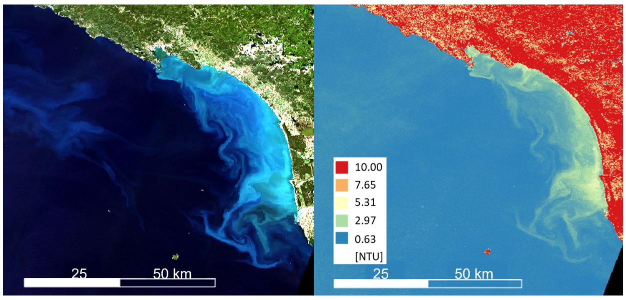

Figure 9. RGB composite and derived turbidity map, relative to 13 October 2021.

4. CONCLUSIONS

Turbidity is an optical property of water, that can affect a variety of aquatic ecosystem processes.
The main aim of this research was to identify a methodology for monitoring sea water turbidity from Sentinel-2 imagery. The need to apply atmospheric correction to older images, of which only the L1C product is available, requires one to focus on the atmospheric correction methods and in particular to the AOD parameter.
The tested software used for the atmospheric correction were QGIS, GRASS GIS and SNAP. While the first one uses an image-based approach (DOS method), the others use a physically-based approach that need to define atmospheric models and parameters, but that allow to apply a better correction. The best atmospheric correction results were obtained with SNAP.

AOD results to be highly variable in space and time, as observed comparing values measured in different AERONET stations. Furthermore, it was found that the AOD value strongly influences the final corrected product with the GRASS module *i.atcorr*, thus also the correlation between the different bands and sea water turbidity.
The visible bands (blue, green and red) have shown a good correlation with the surface reflectance, while NIR bands did not. The best combination between them was found, and a linear model was obtained and tested. Indeed, the estimated satellite-derived surface turbidity had good agreement with the in situ measured turbidity.
In conclusion, the identified EO technique provides a fast and inexpensive monitoring system to observe sea water turbidity along the Northern Tyrrhenian Sea (Italy). On the other hand, the implemented model is highly influenced by the dataset, in particular by its minimum and maximum values. To improve it, a larger number of in situ turbidity measurements is needed, which requires a specific planning of sampling campaigns, that considers the satellite revisit period over the study area of 2-3 days. Additionally, it should be taken into account that high turbidity scenarios often correspond to meteorological events related to high cloudiness, where satellite images have to be excluded. Possible future developments concern the exploration of linear regression models across all the bands, and the possible use of ARPAL and ARPAT in situ data for training and testing nonlinear correlative models through machine learning algorithms. Finally, some test will be carried out to assess the possibility of generalization of the proposed approach beyond the North Tyrrhenian sea.

ACKNOWLEDGEMENTS

Turbidity field data for Liguria and Tuscany coastal areas were provided by the Regional Agency for the Environmental Protection of Liguria (ARPAL) and of Tuscany (ARPAT), that the authors wish to thank.

REFERENCES

Abirhire, O., Davies, J. M., G., X., Hudson, J., 2020. Understanding the factors associated with long-term reconstructed turbidity in Lake Diefenbaker from Landsat-imagery. *Science of The Total Environment*, 724. https://doi.org/10.1016/j.scitotenv.2020.138222.

Akbar, T. A., , Hassan, Q. K., Achari, G., 2014. Development of Remote Sensing Based Models for Surface Water Quality. *CLEAN – Soil, Air, Water*, 42(8), 1044–1051. https://doi.org/10.1002/clen.201300001.

Caballero, I., Steinmetz, F., G., N., 2018. Evaluation of the first year of operational Sentinel-2A data for retrieval of suspended solids in medium- to high-turbidity waters. *Remote Sensing*. https://doi.org/10.3390/rs10070982.

Chavez, P. S., 1988. An improved dark-object subtraction technique for atmospheric scattering correction of multispectral data. *Remote Sensing of Environment*, 24(3), 459–479. https://doi.org/10.1016/0034-4257(88)90019-3.

Chavez, P. S., 1996. Image-Based Atmospheric Corrections - Revisited and Improved. *Photogrammetric Engineering and Remote Sensing*, 62, 1025–1036.

Congedo, L., 2021. Semi-Automatic Classification Plugin: A Python tool for the download and processing of remote sensing images in QGIS. *Journal of Open Source Software*, 6(64). https://doi.org/10.21105/joss.03172.

El Din, E. S., 2021. Enhancing the accuracy of retrieving quantities of turbidity and total suspended solids using Landsat-8-based-principal component analysis technique. *Journal of Spatial Science*, 66(3), 493–512. https://doi.org/10.1080/14498596.2019.1674197.

European Space Agency, 2020. SeNtinel Application Platform (SNAP) ver 8.0.0. http://step.esa.int, last accessed on 25 May 2022.

Gholizadeh, M. H., Melesse, A. M., Reddi, L., 2016. A Comprehensive Review on Water Quality Parameters Estimation Using Remote Sensing Techniques. *Sensors*, 16(8). https://doi.org/10.3390/s16081298.

Giles, D. M., Sinyuk, A., Sorokin, M. G., Schafer, J. S., Smirnov, A., Slutsker, I., Eck, T. F., Holben, B. N., Lewis, J. R., Campbell, J. R., Welton, E. J., Korkin, S. V., Lyapustin, A. I., 2019. Advancements in the Aerosol Robotic Network (AERONET) Version 3 database – automated near-real-time quality control algorithm with improved cloud screening for Sun photometer aerosol optical depth (AOD) measurements. *Atmos. Meas. Tech.*, 12, 169–209. https://doi.org/10.5194/amt-12-169-2019.

GRASS Development Team, 2022a. Geographic Resources Analysis Support System (GRASS) Software. Open Source Geospatial Foundation. grass.osgeo.org last accessed on 25 May 2022.

GRASS Development Team, 2022b. i.atcorr - GRASS GIS MANUAL. Open Source Geospatial Foundation. https://grass.osgeo.org/grass80/manuals/i.atcorr.html last accessed of 25 May 2022.

Hadjimitsis, D. G., Clayton, C. R. I., Hope, V. S., 2004. An assessment of the effectiveness of atmospheric correction algorithms through the remote sensing of some reservoirs. *International Journal of Remote Sensing*, 25(18), 3651–3674. https://doi.org/10.1080/01431160310001647993.

Hafeez, S., Wong, M. S., Abbas, S., Kwok, C. Y. T., Nichol, J., Lee, K. H., Tang, D., Pun, L., 2018. Detection and monitoring of marine pollution using remote sensing technologies. *Monitoring of Marine Pollution*, IntechOpen, Rijeka.

Joshi, I. D., D'Sa, E. J., Osburn, C. L., Bianchi, T. S., 2017. Turbidity in Apalachicola Bay, Florida from Landsat 5 TM and field data: seasonal patterns and response to extreme events. *Remote Sensing*, 9(4). https://doi.org/10.3390/rs9040367.

Kirk, J. T. O., 1985. Effects of suspensoids (turbidity) on penetration of solar radiation in aquatic ecosystems. *Hydrobiologia*, 125(1), 195–208. https://doi.org/10.1007/BF00045935.

Kotchenova, S. Y., Vermote, E. F., Matarrese, R., Klemm, F., 2006. Validation of a vector version of the 6S radiative transfer code for atmospheric correction of satellite data. Part I: Path radiance. *Applied Optics*, 45(26), 6762–6774. https://doi.org/10.1364/AO.45.006762.

Lantzanakis, G., Mitraka, Z., Chrysoulakis, N., 2017. Comparison of physically and image based atmospheric correction methods for Sentinel-2 satellite imagery. *Perspectives on Atmospheric Sciences*, 255–261.

Lee, H., Kim, E. J., Park, S. S., Choi, J. H., 2015. Effects of climate change on the movement of turbidity flow in a stratified reservoir. *Water Resources Management*, 29(11), 4095–4110. https://doi.org/10.1007/s11269-015-1047-2.

Lisi, I., Feola, A., Bruschi, A., Pedroncini, A., Pasquali, D., Risio, M. D., 2019. Mathematical modeling framework of physical effects induced by sediments handling operations in marine and coastal areas. *Journal of Marine Science and Engineering*, 7(149). https://doi.org/10.3390/jmse7050149.

Liu, L., Wang, Y., 2019. Modelling Reservoir Turbidity Using Landsat 8 Satellite Imagery by Gene Expression Programming. *Water*, 11(7). https://doi.org/10.3390/w11071479.

Louis, J., Debaecker, V., Pflug, B., Main-Knorn, M., Bieniarz, J., Mueller-Wilm, U., Cadau, E., Gascon, F., 2016. SENTINEL-2 SEN2COR: L2A Processor for Users.

Moore, G. K., 1980. Satellite remote sensing of water turbidity / Sonde de télémesure par satellite de la turbidité de l'eau. *Hydrological Sciences Bulletin*, 25(4), 407–421. https://doi.org/10.1080/02626668009491950.

Myint, S., Walker, N., 2002. Quantification of surface suspended sediments along a river dominated coast with NOAA AVHRR and SeaWiFS measurements: Louisiana, USA. *International Journal of Remote Sensing*, 23(16), 3229–3249. https://doi.org/10.1080/01431160 110104700.

Nas, B., Ekercin, S., Karabörk, H., Berktay, A., Mulla, D. J., 2010. An Application of Landsat-5TM Image Data for Water Quality Mapping in Lake Beysehir, Turkey. *Water, Air, & Soil Pollution*, 212(1), 183–197. https://doi.org/10.1007/s11270-010-0331-2.

Olds, B. P., Peterson, B. C., Koupal, K. D., Farnsworth-Hoback, K. M., Schoenebeck, C. W., Hoback, W. W., 2011. Water quality parameters of a Nebraska reservoir differ between drought and normal conditions. *Lake and Reservoir Management*, 27(3), 229–234. https://doi.org/10.1080/07438141.2011.601401.

Pereira, L. S. F., Andes, L. C., Cox, A. L., Ghulam, A., 2018. Measuring suspended-sediment concentration and turbidity in the middle Mississippi and lower Missouri Rivers using Landsat data. *JAWRA Journal of the American Water Resources Association*, 54(2), 440–450. https://doi.org/10.1111/1752-1688.12616.

QGIS Development Team, 2022. QGIS Geographic Information System. https://www.qgis.org, last accessed on 25 May 2022.

Quang, N. H., Sasaki, J., Higa, H., Huan, N. H., 2017. Spatiotemporal variation of turbidity based on Landsat 8 OLI in Cam Ranh Bay and Thuy Trieu Lagoon, Vietnam. *Water*, 9(8). https://doi.org/10.3390/w9080570.

Roger, J., Vermote, E., Skakun, S., Murphy, E., Dubovik, O., Kalecinski, N., Korgo, B., Holben, B., 2022. Aerosol models from the AERONET database: application to surface reflectance validation. *Atmospheric Measurement Techniques*, 15(5), 1123–1144. https://doi.org/10.5194/amt-15-1123-2022.

Saberioon, M., Brom, J., Nedbal, V., Soucě, P., Císar, P., 2020. Chlorophyll-a and total suspended solids retrieval and mapping using Sentinel-2A and machine learning for inland waters. *Ecological Indicators*, 113. https://doi.org/10.1016/j.ecolind.2020.106236.

Sagan, V., Peterson, K. T., Maimaitijiang, M., Sidike, P., Sloan, J., Greeling, B. A., Maalouf, S., Adams, C., 2020. Monitoring inland water quality using remote sensing: potential and limitations of spectral indices, bio-optical simulations, machine learning, and cloud computing. *Earth-Science Reviews*, 205. https://doi.org/10.1016/j.earscirev.2020.103187.

Teillet, P. M., 1986. Image correction for radiometric effects in remote sensing. *International Journal of Remote Sensing*, 7(12), 1637–1651. https://doi.org/10.1080/01431168608948958.

Vermote, E., Tanre, D., Deuze, J., Herman, M., Morcette, J., 1997. Second Simulation of the Satellite Signal in the Solar Spectrum, 6S: an overview. *IEEE Transactions on Geoscience and Remote Sensing*, 35(3), 675–686. https://doi.org/10.1109/36.581987.

Wang, F., Han, L., Kung, H., Van Arsdale, R. B., 2006. Applications of Landsat-5 TM imagery in assessing and mapping water quality in Reelfoot Lake, Tennessee. *International Journal of Remote Sensing*, 27(23), 5269-5283. https://doi.org/10.1080/01431160500191704.

Wang, M., Yao, Y., Shen, Q., Gao, H., Li, J., Zhang, F., Wu, Q., 2021. Time-Series Analysis of Surface-Water Quality in Xiong'an New Area, 2016–2019. *Journal of the Indian Society of Remote Sensing*, 49(4), 857–872. https://doi.org/10.1007/s12524-020-01264-8.

Zampoukas, N., Piha, H., Bigagli, E., Hoepffner, N., Hanke, G., Cardoso, A. C., 2013. Marine monitoring in the European Union: how to fulfill the requirements for the marine strategy framework directive in an efficient and integrated way. *Marine Policy*, 39, 349–351. https://doi.org/10.1016/j.marpol.2012.12.004.